https://doi.org/10.20965/jrm.2019.p0143

Paper:

Choice of Muscular Forces for Motion Control of a Robot Arm with Biarticular Muscles

Tetsuya Morizono*, Kenji Tahara, and Hitoshi Kino***

*Fukuoka Institute of Technology
3-30-1 Wajiro-Higashi, Higashi-ku, Fukuoka City, Fukuoka 811-0295, Japan
E-mail: {morizono, kino}@fit.ac.jp
**Kyushu University
744 Moto'oka, Nishi-ku, Fukuoka City, Fukuoka 819-0395, Japan
E-mail: tahara@ieee.org

[Received September 19, 2018; accepted November 28, 2018]

The contribution of biarticular muscles to the control of robotic arms and legs has recently attracted great interest in the field of robotics. The advantages of using biarticular muscles under kinetic interaction with the external environment have been well studied; however, the contribution of the muscles to the motion control of articulated robot arms under no kinetic interaction appears to remain an unclear issue, especially for robot arms of which the muscles are directly anchored to their links, which induces a change in the moment arms to allow the muscles to generate joint torques and permit point-to-point motion control to their desired postures in a feedforward manner with constant muscular forces. This paper presents a case study in which the role of biarticular muscles in the motion control of an articulated robot arm was investigated, focusing on the feature of its redundancy actuation, which allows an arbitrary choice from infinite combinations of muscular forces, realizing motion control to a desired posture. The numerical analysis in this paper addresses three typical combination choices. Mappings from muscular forces to desired postures are calculated in the analysis of the three choices. The simulation results of motion control executed according to the three mappings are also analyzed. The analysis indicates the interesting results that biarticular muscles do not contribute to the desired postures and that a very weak dependence property of monoarticular muscles on the desired postures exists for a particular choice. The simulation results also demonstrate that the implementation of one choice results in a degraded motion control performance as compared with that of the two other choices.

Keywords: robot arm, redundant actuation, biarticular muscle, point-to-point control, binocular visual space

1. Introduction

Robot arms and legs that reflect the musculoskeletal structure of human limbs in their mechanical designs have recently received considerable attention in the field of robotics, with the expectation that their features will allow the implementation of advanced control techniques to improve their motion performance. In their mechanical design, special attention is sometimes paid to the existence of biarticular muscles, such as the biceps brachii and triceps brachii muscles in the case of a human arm, which are anchored to both adjacent joints and actuate these joints simultaneously.

A previous study showed that an advantageous effect of biarticular muscles is obtained by coupling the knee and ankle joints of a robotic leg by a wire representing a biarticular muscle (a gastrocnemius) with appropriate timing [1]. The advantage of coupling the two joints by a biarticular muscle to facilitate the jumping performance of a robotic leg was also shown experimentally [2]. Additional studies addressed the control problems related to robotic legs, including the impact upon landing on the ground [3, 4]. This impact transmits a very high frequency mechanical oscillation to the legs, and its wide frequency bandwidth renders sensory feedback control difficult, because the signal bandwidth of the feedback is in general limited. To overcome the control difficulty, motion control of the legs at impact by controlling their stiffness ellipsoids at their endtip was proposed; the biarticular muscles played a key role in these proposed methods.

Motion control of robot arms by biarticular muscles was also addressed in many studies. A study examining the hybrid position/force control of a 2-degrees of freedom (DOFs) planar robot arm obtained the result that the direction of the interaction force between an object and the endtip of the robot arm can be kept constant irrespective of the changes in the posture of the robot arm [5]. It is interesting that this result suggests that explicit control to determine the direction of the interaction force is unnecessary, and the effort necessary for controlling the robot arm can be reduced by using biarticular muscles. A study also exists that was focused on the actuation redundancy

© Fuji Technology Press Ltd. Creative Commons CC BY-ND: This is an Open Access article distributed under the terms of the Creative Commons Attribution-NoDerivatives 4.0 International License (http://creativecommons.org/licenses/by-nd/4.0/).

provided by the addition of biarticular muscles. The redundancy means that the control inputs to the muscles for actuation of the robot arm cannot be uniquely determined; this is considered a disadvantageous aspect of the redundancy. However, this aspect also allows the robot arm to accept different control input combinations for the same desired posture, according to the requirements for the control, such as actuator output limits [6–8].

A major model of the robot arm with biarticular muscles is the *pulley* model [6, 7, 9, 10]. In this model, the joints in the robot arm have pulleys and tendons connected (or anchored) to the pulleys, and the actuation of the joints is executed by pulling the tendons with muscle type actuators. In contrast, some authors have focused on the *non-pulley* model [11], which has no pulleys on the joints. In this model, tendons actuated by muscle type actuators are directly anchored to the links of the robot arm. An interesting feature of this model is that the point-to-point (PTP) motion control of the robot arm to a desired posture can be realized by the "balance" of the muscular forces, if the muscular arrangement of the robot arm satisfies a stability condition for motion control [11]. This means that no spring element is required for creating an equilibrium point in the posture of the robot arm, as implemented in the robot arm with pulley model, and only application of the muscular forces is required to achieve posture control of the robot arm. The muscular forces can be kept constant; therefore, *feedforward* PTP control to a desired posture is also possible. In addition, a recent study demonstrated that feedforward control contributes to suppressing the unstable behavior of the robot arm, even when the sensory feedback used for the control includes a time delay [12].

The motivation of the studies mentioned above was the hope or expectation that a performance improvement in robot arm or leg control can be achieved by incorporating biarticular muscles (or equivalent linear actuation units or linkages) in robots. This is also true for robots that interact with an external environment, such as robot legs jumping under interaction with a floor or robot arms pushing an object in an external environment with their endtips. The incorporation of biarticular muscles in robot arms or legs improves motion performance, overcomes control difficulties, and reduces the effort necessary for control [13]. However, the intrinsic contribution of biarticular muscles in the case of motion control where no physical interaction is involved remains unclear, especially as pertains to the non-pulley model of a robot arm.

Biarticular muscles are expected to contribute to motion control, even in the case of motion control without physical interaction; however, actuation of an antagonistically actuated robot arm is also possible *only* by the *monoarticular muscles* in principle, which suggests that the existence of biarticular muscles is non-essential for motion control. This is the issue considered in this paper. In case studies conducted to address the issue, the authors observed that the existence of biarticular muscles can be considered advantageous for improving the performance of PTP feedforward motion control of a robot arm to a desired posture; however, it was also observed that, when one of the choices of muscular forces was applied, the biarticular muscles contributed less to the improvement of the control performance [14, 15]. The determination of the reason for these observations remains an important issue.

The study presented in this paper considered the issue through an analysis using the numerical calculation and simulation results of motion control for a robot arm antagonistically actuated by both monoarticular and biarticular muscles. The remainder of this paper is organized as follows. Section 2 describes the robot arm considered in this paper and gives the definitions of certain Cartesian coordinate frames used there. In Section 3, the calculation of muscular forces for control of the robot arm to its desired posture is described, after a brief explanation of certain static equations used for the calculation. In Section 3, it is assumed that a desired posture of the robot arm is expressed by its desired joint angles; however, Section 4 considers the conversion of this expression to variables defined in the *binocular visual space*. This conversion is motivated by an interest in the sensory-motor coordination performed by human beings, the focus of which is on mapping the desired postures of the robot arm to muscular forces in the binocular visual space. Noting that PTP feedforward motion control to a desired posture can be realized by infinite combinations of muscular forces because of the nature of redundancy and that the choice of the combination is determined by an arbitrarily determined vector in the calculation of the muscular forces, Section 5 considers three typical choices for the vector and shows the calculation results of muscular forces for these three vectors. An interesting observation presented in this section is that the results show almost the same dependency of the muscular forces on the desired posture for two of the three choices and almost *no* (or a very weak) dependency for the third choice. It is also observed that in the third vector choice the biarticular muscles make no contribution at the desired postures. Based on these observations, Section 6 assumes a relation between the control performance and dependencies, and this assumption is investigated through the simulation results presented in Section 7. Section 8 concludes the discussion in this paper and describes a future vision from an engineering viewpoint and some future issues related to the study in this paper.

2. Model of the Robot Arm

2.1. Muscles and Links

A two DOF planar robot arm is addressed in this paper, the muscular and link arrangement of which is shown in **Fig. 1(a)**. Here, it is assumed that the motion of the robot arm occurs in a horizontal plane; hence, it is assumed that no gravitational effect is exerted on the robot arm. The robot has three links, labeled links 0, 1, and 2. Link 0 is the base link, which is assumed to be immobile (anchored

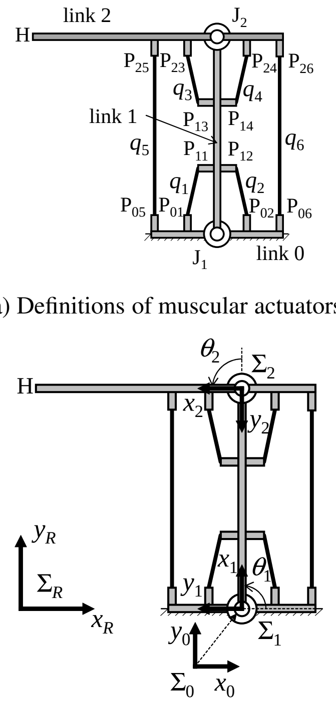

(a) Definitions of muscular actuators

(b) Definitions of coordinate frames

Fig. 1. Definitions of muscles and coordinate frames of the robot arm.

to a fixed floor, for example). Link 1 is connected to link 0 by a rotational joint, J_1, and link 2 is also connected to link 1 by a second rotational joint, J_2. Point H denotes the distal endtip of the robot arm.

However, the robot arm has six muscular or linear type actuators (referred to as muscle i $(i = 1, \ldots, 6)$ hereinafter), and the actuators are anchored to the points on the links. Each link has four anchoring points. The first letter m of the subscript in the point label P_{mn} denotes the link number, whereas the second letter n denotes the muscle number; for example, P_{01} indicates the anchoring point of muscle 1 on link 0.

The length of muscle i is denoted by q_i. Muscles 1 and 2 are monoarticular muscles antagonistically actuating J_1. Similarly, muscles 3 and 4 are those actuating J_2. On the other hand, muscles 5 and 6 are biarticular muscles actuating both joints simultaneously. The structure of the model shown in **Fig. 1** is rather simplified in comparison with that of a human arm; however, this simplification considers the mechanical design and manufacture of the robot arm for experiments planned in the future.

2.2. Coordinate Frames

For expressing robot movement, four Cartesian coordinate frames are defined, as shown in **Fig. 1(b)**. The coordinate frame Σ_R is the reference coordinate frame for expressing the positional coordinate values of point H. Σ_m $(m = 0,\ 1,\ 2)$ presents the link frames for link m. The origins of Σ_0 and Σ_1 are located at the same position on the rotational axis of J_1. The origin of Σ_2 is located on the rotational axis of J_2.

The directions of the coordinate frame axes are determined so that the Denavit-Hartenberg notation is applicable to the entire robot arm; therefore, the joint angles θ_p $(p = 1,\ 2)$ of J_p are expressed by the rotational angles from the axes x_{p-1} to x_p.

3. Point-To-Point Feedforward Motion Control

3.1. Relation Between Muscular Forces and Joint Torques

With the definitions of α_i and τ_p for the forces of muscle i and the joint torques of J_p, the following equation holds.

$$\boldsymbol{\tau} = \boldsymbol{W}(\boldsymbol{\theta})\,\boldsymbol{\alpha}, \qquad (1)$$

where $\boldsymbol{\tau} = [\ \tau_1 \quad \tau_2\ ]^T$ and $\boldsymbol{\alpha} = [\ \alpha_1 \ \cdots \ \alpha_6\ ]^T$. $\boldsymbol{W}(\boldsymbol{\theta})$ is the 2×6 matrix mapping $\boldsymbol{\alpha}$ to $\boldsymbol{\tau}$ dependent on the joint angle vector $\boldsymbol{\theta} = [\ \theta_1 \quad \theta_2\ ]^T$ and satisfies the kinematic relation

$$\dot{\boldsymbol{q}} = \boldsymbol{W}^T(\boldsymbol{\theta})\,\dot{\boldsymbol{\theta}}, \qquad (2)$$

where $\dot{\boldsymbol{q}} = [\ \dot{q}_1 \ \cdots \ \dot{q}_6\ ]^T$ is the vector expressing the changing rate of the muscular lengths, and $\dot{\boldsymbol{\theta}}$ is the angular velocity vector of the joints.

From Eq. (1), $\boldsymbol{\alpha}$ is calculated from $\boldsymbol{\tau}$ by

$$\boldsymbol{\alpha} = \boldsymbol{W}^+(\boldsymbol{\theta})\,\boldsymbol{\tau} + \left\{\boldsymbol{I}_6 - \boldsymbol{W}^+(\boldsymbol{\theta})\,\boldsymbol{W}(\boldsymbol{\theta})\right\}\boldsymbol{k}_e, \qquad (3)$$

where $\boldsymbol{W}^+(\boldsymbol{\theta}) = \boldsymbol{W}^T(\boldsymbol{\theta})\{\boldsymbol{W}(\boldsymbol{\theta})\boldsymbol{W}^T(\boldsymbol{\theta})\}^{-1}$ is the pseudo-inverse matrix of $\boldsymbol{W}(\boldsymbol{\theta})$ (6×2 matrix), $\boldsymbol{I}_6$ is the 6×6 identity matrix, and $\boldsymbol{k}_e$ is the vector that can be arbitrarily chosen.

3.2. Basic Idea of Feedforward Control by Muscular Forces

If no joint torque is assumed, the substitution of $\boldsymbol{\tau} = \boldsymbol{0}$ into Eq. (3) yields

$$\boldsymbol{\alpha} = \left\{\boldsymbol{I}_6 - \boldsymbol{W}^+(\boldsymbol{\theta})\,\boldsymbol{W}(\boldsymbol{\theta})\right\}\boldsymbol{k}_e. \qquad (4)$$

As mentioned in the previous subsection (Section 3.1), $\boldsymbol{k}_e$ is arbitrary; therefore, we can assume a constant vector for $\boldsymbol{k}_e$. In this case, it is understood from Eq. (4) that $\boldsymbol{\alpha}$ is dependent only on $\boldsymbol{\theta}$.

If we have a desired posture of the robot arm and the posture is expressed by a desired joint angle vector $\boldsymbol{\theta}_d = [\ \theta_{d1} \quad \theta_{d2}\ ]^T$, then the muscular forces at the desired posture $\boldsymbol{v}(\boldsymbol{\theta}_d)$ is calculated by

$$\boldsymbol{v}(\boldsymbol{\theta}_d) = \left\{\boldsymbol{I}_6 - \boldsymbol{W}^+(\boldsymbol{\theta}_d)\,\boldsymbol{W}(\boldsymbol{\theta}_d)\right\}\boldsymbol{k}_e. \qquad (5)$$

By substituting $\boldsymbol{v}(\boldsymbol{\theta}_d)$ in Eq. (5) into $\boldsymbol{\alpha}$ in Eq. (1) under the condition $\boldsymbol{\theta} = \boldsymbol{\theta}_d$, $\boldsymbol{\tau}$ becomes the zero vector, and it is understood that $\boldsymbol{v}(\boldsymbol{\theta}_d)$ generates no joint torques at the desired posture. This means that $\boldsymbol{v}(\boldsymbol{\theta}_d)$ does not need to be modified, even after the arrival of the robot arm at the desired posture. In addition, the joint torques necessary to

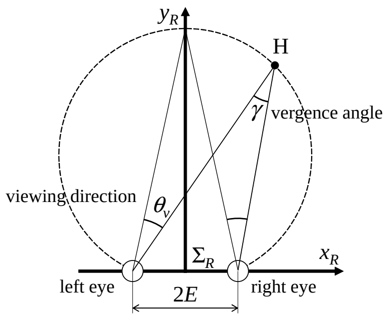

Fig. 2. Binocular visual space.

allow the robot arm to approach a desired posture are generated when the joint angles θ_1 and θ_2 do not reach their desired angles θ_{d1} and θ_{d2}, because $\boldsymbol{\tau} = \boldsymbol{W}(\boldsymbol{\theta})\boldsymbol{v}(\boldsymbol{\theta}_d) \neq \boldsymbol{0}$ when $\boldsymbol{\theta} \neq \boldsymbol{\theta}_d$.

From the above, it is understood that the muscular forces in $\boldsymbol{v}(\boldsymbol{\theta}_d)$ calculated by Eq. (5) can actuate the robot arm to a given desired posture $\boldsymbol{\theta}_d$ from an initial posture $\boldsymbol{\theta}_0 \neq \boldsymbol{\theta}_d$. It is also understood that this PTP motion control is performed in a feedforward manner, as the calculation of $\boldsymbol{v}(\boldsymbol{\theta}_d)$ by Eq. (5) does not require any feedback information on the posture of the robot arm (expressed by a joint angle vector $\boldsymbol{\theta}$) during the control term.

4. Introduction of Binocular Visual Space

A desired posture of the robot arm can be expressed by the following description methods: the use of the joint angles described in the previous subsection (Section 3.2) is one of the methods. The use of the coordinate values of the endtip of the robot arm (point H in **Fig. 1**) in the reference coordinate frame Σ_R is an another description method; however, this section considers the expression of the desired posture in the binocular visual space.

In the binocular visual space depicted in **Fig. 2**, the location of the endtip of the robot arm (point H in **Fig. 2**) is expressed by two variables: the viewing direction θ_v and the vergence angle γ. Two "eyes" on the x_R-axis are axisymmetrically arranged on the y_R-axis. The distance between the eyes is $2E$, where E is a positive constant. The vergence angle γ is the circumferential angle between the two lines to the left and right eyes at point H. The viewing direction θ_v is the angle between the line from the left or right eye to point H and the line from the eye to the point where the circumference of the Vieth-Müller circle intersects the y_R-axis. The angles of the viewing direction to point H of the two eyes are the same.

The calculation of the coordinate values ${}^R x_H$ and ${}^R y_H$ of point H in Σ_R from a given set of γ and θ_v follows

$$ {}^R x_H = \frac{E \sin 2\theta_v}{\sin\gamma}, \quad \ldots \quad (6)$$

$$ {}^R y_H = \frac{E\left(\cos 2\theta_v + \cos\gamma\right)}{\sin\gamma}. \quad \ldots \quad (7)$$

If we introduce the vector expressing the variables in the binocular visual space $\boldsymbol{b} = [\ \theta_v \quad \gamma\ ]^T$ and the position vector ${}^R\boldsymbol{p}_H = [\ {}^R x_H \quad {}^R y_H\ ]^T$ in Σ_R, Eqs. (6) and (7) can be expressed in a vector form:

$$ {}^R\boldsymbol{p}_H(\boldsymbol{b}) = \boldsymbol{f}_b^p(\boldsymbol{b}) = \begin{bmatrix} f_{xH}(\boldsymbol{b}) \\ f_{yH}(\boldsymbol{b}) \end{bmatrix}, \quad \ldots \quad (8)$$

where $\boldsymbol{f}_b^p(\boldsymbol{b})$ means a mapping function of $\boldsymbol{b}$ from the binocular visual space to the space by Σ_R, and $f_{xH}(\boldsymbol{b})$ and $f_{yH}(\boldsymbol{b})$ in Eq. (8) correspond to Eqs. (6) and (7), respectively.

An expression similar to Eq. (8) can be applied for the inverse kinematics of the robot arm in **Fig. 1** from the coordinate values of point H in Σ_R to the joint angles as follows: $\boldsymbol{\theta}({}^R\boldsymbol{p}_H) = \boldsymbol{f}_p^\theta({}^R\boldsymbol{p}_H)$; therefore, the following equation holds for a desired posture of the robot arm given by vector $\boldsymbol{b}_d = [\ \theta_{vd} \quad \gamma_d\ ]^T$ in the binocular visual space:

$$ \boldsymbol{\theta}_d = \boldsymbol{\theta}(\boldsymbol{b}_d) = \boldsymbol{\theta}\left({}^R\boldsymbol{p}_H(\boldsymbol{b}_d)\right). \quad \ldots \quad (9)$$

By substituting $\boldsymbol{\theta}_d$ in Eq. (9) into Eq. (5), the mapping from $\boldsymbol{b}_d$ to $\boldsymbol{v}(\boldsymbol{\theta}_d)$ is obtained.

5. Numerical Analysis

5.1. Choices of the Arbitrary Vector

As mentioned in the previous section (Section 4), $\boldsymbol{k}_e$ in Eq. (5) for the calculation of $\boldsymbol{v}(\boldsymbol{\theta}_d)$ is the arbitrarily chosen vector. An example of the choice was proposed by some authors in [11] based on the criterion of minimizing the Euclidean norm of $\boldsymbol{v}(\boldsymbol{\theta}_d)$; however, in this study we considered the following three choices:

$$ \boldsymbol{k}_{ea} = [\ 1 \quad 1 \quad 1 \quad 1 \quad 1 \quad 1\ ]^T, \quad \ldots \quad (10)$$

$$ \boldsymbol{k}_{e56} = [\ 0 \quad 0 \quad 0 \quad 0 \quad 1 \quad 1\ ]^T, \quad \ldots \quad (11)$$

$$ \boldsymbol{k}_{e14} = [\ 1 \quad 1 \quad 1 \quad 1 \quad 0 \quad 0\ ]^T. \quad \ldots \quad (12)$$

The purpose of the above choices was to inspect how the column vectors in $\boldsymbol{I}_6 - \boldsymbol{W}^+(\boldsymbol{\theta}_d)\boldsymbol{W}(\boldsymbol{\theta}_d)$ in Eq. (5) contribute to the mapping from the desired postures to muscular forces at the postures. The column vectors in the matrix can be explicitly written as

$$ \begin{aligned} &\boldsymbol{I}_6 - \boldsymbol{W}^+(\boldsymbol{\theta}_d)\boldsymbol{W}(\boldsymbol{\theta}_d) \\ &\quad = [\ \boldsymbol{w}_1(\boldsymbol{\theta}_d) \quad \boldsymbol{w}_2(\boldsymbol{\theta}_d) \quad \cdots \quad \boldsymbol{w}_6(\boldsymbol{\theta}_d)\ ], \quad . \quad (13) \end{aligned}$$

where $\boldsymbol{\theta}_d$ can be replaced with $\boldsymbol{b}_d$ by using Eq. (9).

Substituting each of the three vectors given in Eqs. (10)–(12) into $\boldsymbol{k}_e$ in Eq. (5) yields

$$ \boldsymbol{w}_1(\boldsymbol{b}_d) + \cdots + \boldsymbol{w}_6(\boldsymbol{b}_d) = \boldsymbol{w}_a(\boldsymbol{b}_d) = \boldsymbol{w}_{da} \text{ for } \boldsymbol{k}_{ea}, \quad (14)$$

$$ \boldsymbol{w}_5(\boldsymbol{b}_d) + \boldsymbol{w}_6(\boldsymbol{b}_d) = \boldsymbol{w}_{56}(\boldsymbol{b}_d) = \boldsymbol{w}_{d56} \text{ for } \boldsymbol{k}_{e56}, \quad . \quad (15)$$

$$ \begin{aligned} \boldsymbol{w}_1(\boldsymbol{b}_d) + \cdots + \boldsymbol{w}_4(\boldsymbol{b}_d) &= \boldsymbol{w}_{14}(\boldsymbol{b}_d) \\ &= \boldsymbol{w}_{d14} \text{ for } \boldsymbol{k}_{e14}. \quad \ldots \quad (16) \end{aligned}$$

Here, $\boldsymbol{w}_{da} = \boldsymbol{w}_{d14} + \boldsymbol{w}_{d56}$, and therefore, we can investigate how each of the combinations of $\boldsymbol{w}_1(\boldsymbol{b}_d) + \cdots +$

$\boldsymbol{w}_4(\boldsymbol{b}_d)$ and $\boldsymbol{w}_5(\boldsymbol{b}_d)+\boldsymbol{w}_6(\boldsymbol{b}_d)$ contribute to the determination of $\boldsymbol{v}(\boldsymbol{\theta}_d)$.

Antagonistically actuated robot arms, as shown in **Fig. 1**, sometimes use tendon-driven actuation systems with cables. In this case, motion control of the robot requires the condition that all the muscular forces are *positive* at every desired posture to prevent the cables becoming loose at the posture. However, the focus of the discussion in this paper is on investigating the contribution of the combinations $\boldsymbol{w}_1(\boldsymbol{b}_d)+\cdots+\boldsymbol{w}_4(\boldsymbol{b}_d)$ and $\boldsymbol{w}_5(\boldsymbol{b}_d)+\boldsymbol{w}_6(\boldsymbol{b}_d)$ to mapping from $\boldsymbol{b}_d$ to $\boldsymbol{v}(\boldsymbol{\theta}_d)$, as mentioned in the previous paragraph. Realizing motion control to a desired posture with positive muscular forces is of less interest in this paper. Accordingly, the following discussion accepts *negative* muscular forces (namely, one or more muscular forces in $\boldsymbol{v}(\boldsymbol{\theta}_d)$ are negative) at the desired postures; however, this is naturally an acceptable condition based on the assumption that a type of linear actuator (without a tendon, such as a cable) is used as a muscle in the robot arm.

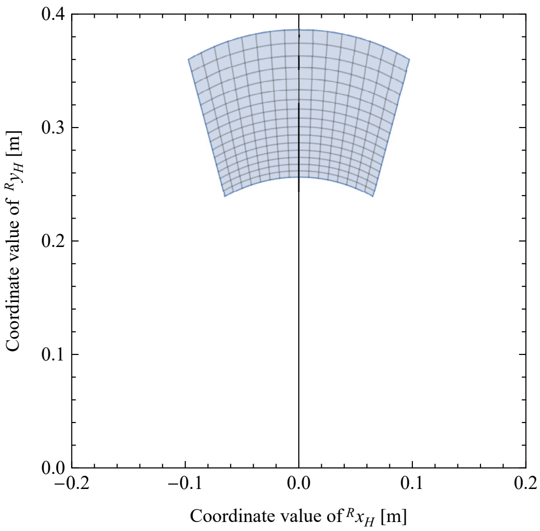

Fig. 3. Calculation range of $\boldsymbol{b}_d$ for analysis illustrated in Σ_R.

5.2. Parameters and Calculation Range for Analysis

The analysis in this paper assumes that the size of the robot arm is similar to that of a human arm. Based on this assumption, the length L_1 of link 1 connecting joint J_2 to joint J_1 in **Fig. 1** is assumed to be 0.3130 m, and the length L_2 of link 2 connecting endtip point H to joint J_2 in **Fig. 1** is assumed to be 0.2516 m. In addition, it is assumed that the origins of the coordinate frames Σ_0 and Σ_1 are located at the position of the coordinate value $(X_{J0},0)$ in Σ_R, where $2X_{J0}=0.3975$ m. Additionally, the distance between the two eyes constituting the binocular visual space, $2E$, is assumed to be 0.0619 m.

These parameter values refer to the average body size of Japanese males [a]. The purpose of using these reference sizes is to gain an insight into sensory-motor coordination between the binocular visual space and the muscular forces when the kinematic size of the robot arm is similar to that of a human arm and the size of the binocular visual space is similar to that constituted by a pair of human eyes. An expectation from this insight is that a feature useful for the PTP control of the robot arm will be found in the mapping from a desired posture expressed in the binocular visual space to the muscular forces.

The range of θ_{vd} is assumed to be from $-\pi/12$ rad to $+\pi/12$ rad and that of γ_d from 0.16 rad to 0.24 rad. These ranges can be illustrated in Σ_R, as shown in **Fig. 3**. The ranges were determined based on the consideration of the field of tabletop work used by a human worker.

The numerical calculation of the muscular forces also requires that the anchoring points of the muscles be defined. The coordinate values of the anchoring points P_{01}, P_{02}, P_{05}, and P_{06} are $(-0.05,0.02)$, $(0.05,0.02)$, $(-0.05,0.02)$, and $(0.05,0.02)$ in Σ_0, respectively. Similarly, those of P_{11}, P_{12}, P_{13}, and P_{14} are $(0.12,0.01)$, $(0.12,-0.01)$, $(0.18,0.01)$, and $(0.18,-0.01)$ in Σ_1, and those of P_{23}, P_{24}, P_{25}, and P_{26} are $(0.05,0.02)$, $(-0.05,0.02)$, $(0.05,0.02)$, and $(-0.05,0.02)$ in Σ_2, respectively. Unfortunately, no reference that provides a suggestion for assuming the above coordinate values of the anchoring points based on a human arm could be found in the literature survey conducted by the authors; however, these coordinate values are determined based on a related previous study of the authors [15].

5.3. Observation of $\boldsymbol{w}_{da}$

The calculation results of $\boldsymbol{w}_{da}$ are shown in **Fig. 4**. The five graphs in the left hand column (subcaptioned (a) at the bottom) show the plots for w_{dai} $(i=1,\ldots,4)$, and those in the right hand column (subcaptioned (b) at the bottom) show the plots for w_{da5} and w_{da6}, where $\boldsymbol{w}_{da}=[\ w_{da1}\ \cdots\ w_{da6}\ ]^T$. The five rows of the graphs in **Fig. 4** correspond to the desired vergence angles $\gamma_d=$ 0.16, 0.18, 0.20, 0.22, and 0.24 rad from the top row. The horizontal axis in each graph denotes the desired viewing direction θ_{vd} [rad], and the vertical axis denotes the value of the muscular forces. The calculation and plotting of the graphs were performed using Wolfram Mathematica® 10.0.1.0.

A major observation is obtained from **Fig. 4(b)**: w_{da5} and w_{da6} exhibit approximately no (or a very weak) dependence property on both θ_{vd} and γ_d. They remain at the constant force of approximately 1.0 N throughout the calculation range. A second observation is the dependence properties of w_{dai} $(i=1,\ldots,4)$ on both θ_{vd} and γ_d: w_{da1} and w_{da4} have almost the same dependency, and their dependencies on θ_{vd} are negative. w_{da2} and w_{da3} also have almost the same dependency; however, their dependencies on θ_{vd} are positive. In addition, the dependence properties described above seem to be almost linear, at least in the calculation range considered in this paper. Comparisons of the graphs in the left hand column also lead to the observation that the dependence properties on θ_{vd} change according to the value of γ_d.

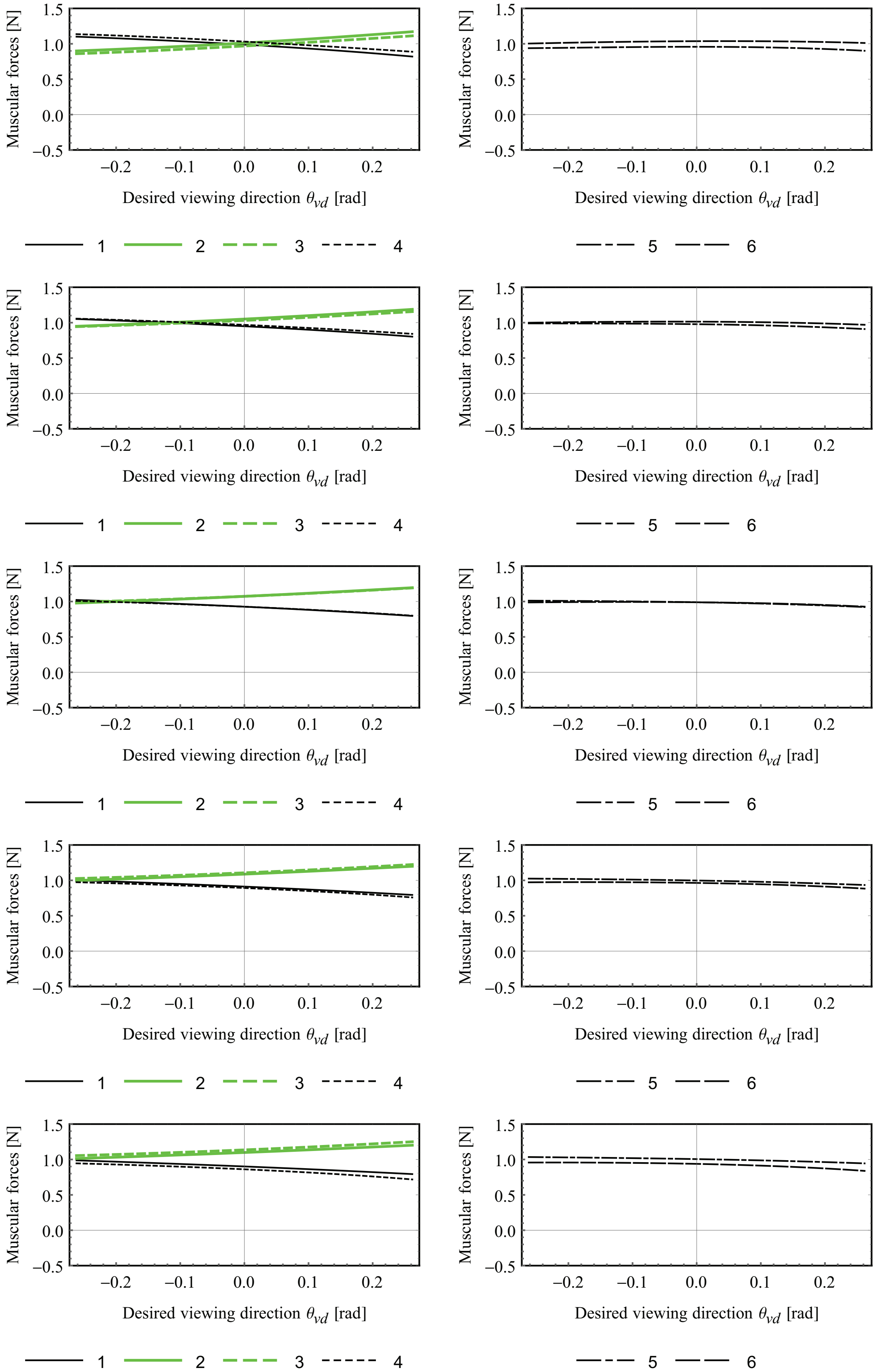

(a) Muscular forces of muscles 1 to 4

(b) Muscular forces of muscles 5 and 6

Fig. 4. Muscular forces according to $\boldsymbol{w}_{da}$ (at $\gamma_d = 0.16$, 0.18, 0.20, 0.22, and 0.24 from the top row of the graphs).

5.4. Observation of $\boldsymbol{w}_{d56}$

The calculation results of $\boldsymbol{w}_{d56}$ are shown in **Fig. 5**, where the graphs are arranged as in **Fig. 4**. The significant observations from **Figs. 4** and **5** are that 1) the muscular forces of muscles 5 and 6 shown in the graphs in the right hand columns of both figures are the same, and 2) the muscular forces of muscles i $(i = 1,\dots,4)$ in the left hand column of both figures have the same dependence properties on θ_{vd} and γ_d; however, the muscular forces in **Fig. 5** are approximately 1 N smaller than those in **Fig. 4**. Since $\boldsymbol{w}_{da} = \boldsymbol{w}_{d56} + \boldsymbol{w}_{d14}$, as mentioned in Section 5.1, these two observations suggest the following: 1) the muscular forces of muscles 5 and 6 are determined only by $\boldsymbol{w}_5(\boldsymbol{b}_d) + \boldsymbol{w}_6(\boldsymbol{b}_d)$ $(= \boldsymbol{w}_{d56})$, and 2) the dependencies of the muscular forces of muscles i $(i = 1,\dots,4)$ on θ_{vd} and γ_d also come only from $\boldsymbol{w}_5(\boldsymbol{b}_d)+\boldsymbol{w}_6(\boldsymbol{b}_d)$. In other words, $\boldsymbol{w}_1(\boldsymbol{b}_d) + \boldsymbol{w}_2(\boldsymbol{b}_d) + \boldsymbol{w}_3(\boldsymbol{b}_d) + \boldsymbol{w}_4(\boldsymbol{b}_d)$ $(= \boldsymbol{w}_{d14})$ does not contribute to 1) the generation of the muscular forces of muscles 5, 6, and 2) the dependence of the muscular forces of muscles i $(i = 1,\dots,4)$ on θ_{vd} and γ_d. The validity of these suggestions is verified in the next subsection.

5.5. Observation of $\boldsymbol{w}_{d14}$

The calculation results of $\boldsymbol{w}_{d14}$ are shown in **Fig. 6**, where the graphs are arranged as in **Figs. 4** and **5**. The graphs in the right hand column of **Fig. 6** show approximately zero constant muscular forces for muscles 5 and 6 throughout the calculation range, and the graphs in the left hand column of **Fig. 6** also show approximately 1 N constant muscular forces for muscle i $(i = 1,\dots,4)$ throughout the range, with little differences from 1 N at $\theta_{vd} = +\pi/12$, as shown in **Table 1**.

The former indicates no contribution of $\boldsymbol{w}_{d14} = \boldsymbol{w}_1(\boldsymbol{b}_d)+\cdots+\boldsymbol{w}_4(\boldsymbol{b}_d)$ to the generation of the muscular forces of the biarticular muscles, and the latter means that $\boldsymbol{w}_{d14}$ does not contribute to the dependence of the muscular forces of muscle i $(i = 1,\dots,4)$ on θ_{vd} and γ_d.

The observations described above are coincident with the suggestions in the previous subsection (Section 5.4). An interesting result obtained from the former observation in the previous paragraph is that the muscular structure of the robot arm at a desired posture is equivalent to that *only* with *monoarticular* muscles when $\boldsymbol{w}_{d14} = \boldsymbol{w}_1(\boldsymbol{b}_d)+\cdots+\boldsymbol{w}_4(\boldsymbol{b}_d)$ is adopted for determining $\boldsymbol{v}(\boldsymbol{\theta}_d)$. This is because the biarticular muscles (muscles 5 and 6, in particular) provide no muscular forces with the robot arm at this posture.

6. Simulation of Motion Control

6.1. Issue on Motion Control

The numerical analysis in Section 5, reveals the results.

- The mappings from $\boldsymbol{b}_d$ to $\boldsymbol{v}(\boldsymbol{\theta}_d)$ obtained by $\boldsymbol{w}_{da} = \boldsymbol{w}_1(\boldsymbol{b}_d)+\cdots+\boldsymbol{w}_6(\boldsymbol{b}_d)$ and $\boldsymbol{w}_{d56} = \boldsymbol{w}_5(\boldsymbol{b}_d)+\boldsymbol{w}_6(\boldsymbol{b}_d)$ exhibit the same dependence properties on θ_{vd} and γ_d, except for the magnitudes of the muscular forces of muscles i $(i = 1,\dots,4)$, and
- A noticeable dependence on θ_{vd} and γ_d is not observed in the mapping using $\boldsymbol{w}_{d14} = \boldsymbol{w}_1(\boldsymbol{b}_d)+\cdots+\boldsymbol{w}_4(\boldsymbol{b}_d)$.

The former result means that $\boldsymbol{v}(\boldsymbol{\theta}_d)$ that realizes a desired posture is uniquely determined from $\boldsymbol{b}_d$ expressing the desired posture; therefore, it can be naturally assumed that the uniqueness of the mapping from $\boldsymbol{b}_d$ to $\boldsymbol{v}(\boldsymbol{\theta}_d)$ produces a (probably advantageous) effect on motion control to the desired posture. In addition, it is expected that the same or very similar performances are obtained from both controls using $\boldsymbol{w}_{da}$ and $\boldsymbol{w}_{d56}$ because of the same dependence properties in the mappings using these vectors.

However, the latter result indicates the necessity that motion control to all the desired postures (in the ranges considered in the numerical analysis) is realized by almost the same $\boldsymbol{v}(\boldsymbol{\theta}_d)$ because of the very slight uniqueness of the mapping by $\boldsymbol{w}_{d14}$. It is assumed that this necessity brings a difficult or disadvantageous effect to the motion control to the desired postures.

According to the consideration described above, this section focuses on a comparison of control performances for the three choices for $\boldsymbol{k}_e$ described in Section 5.1.

6.2. Kinetic Parameters of the Robot Arm

The values of the kinetic parameters used in the simulation are summarized in **Table 2**. The values in the table were calculated based on the average ratios of the upper arms and forearms among Japanese young males [16], assuming that the mass of the entire body was 60 kg.

6.3. Muscular Forces During Control

A damping effect is necessary for stable convergence of the robot arm to a desired posture, in addition to the muscular forces $\boldsymbol{v}(\boldsymbol{\theta}_d)$ for realizing feedforward PTP control; therefore, the muscular forces during control of the robot arm are given by

$$\boldsymbol{\alpha} = \boldsymbol{v}(\boldsymbol{\theta}_d) - \boldsymbol{D}\dot{\boldsymbol{q}}, \qquad (17)$$

where $\boldsymbol{D} = D\boldsymbol{I}_6$ is the matrix of damping coefficients, and the given conditions for D are detailed in the next section (Section 7).

Simulation of the PTP controls was executed on Matlab® and Simulink® (R2016a) software. The choice of the solver in Simulink was ode45 (Dormani-Prince) with a variable time step; however, the maximum time step was limited to 1 ms.

7. Simulation Results and Observation

7.1. Initial Posture and Desired Postures

This paper considers 25 desired postures in the calculation range explained in Section 5.2. These postures are given by combinations of variable values $\theta_{vd} = (-\pi/12, -\pi/24, 0, +\pi/24, +\pi/12)$ rad and $\gamma_d = (0.16, 0.18, 0.20, 0.22, 0.24)$ rad. The endtip positions at these postures plotted in Σ_R are shown in **Fig. 7**

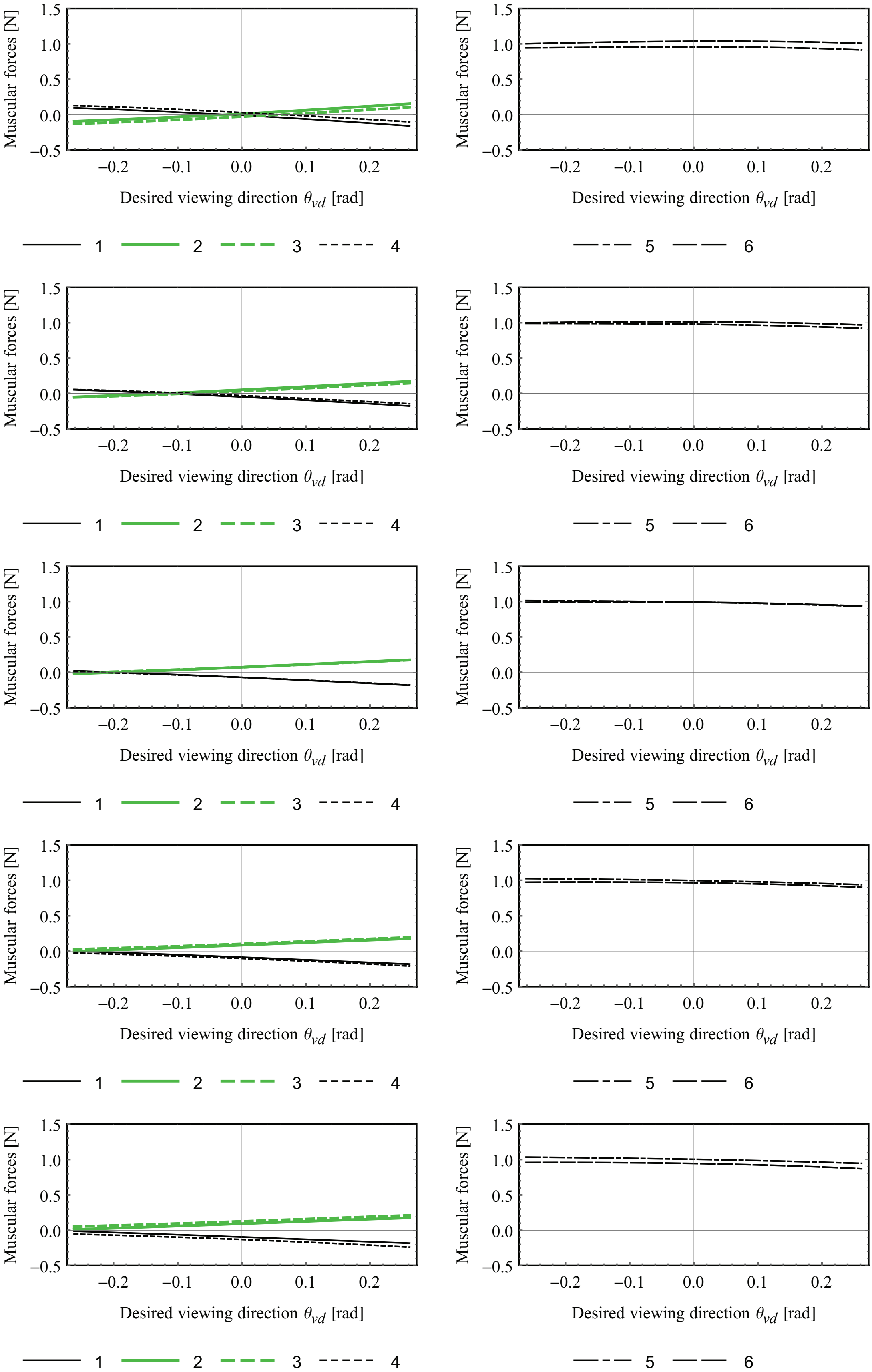

(a) Muscular forces of muscles 1 to 4

(b) Muscular forces of muscles 5 and 6

Fig. 5. Muscular forces according to $\boldsymbol{w}_{d56}$ (at $\gamma_d = 0.16$, 0.18, 0.20, 0.22, and 0.24 from the top row of the graphs).

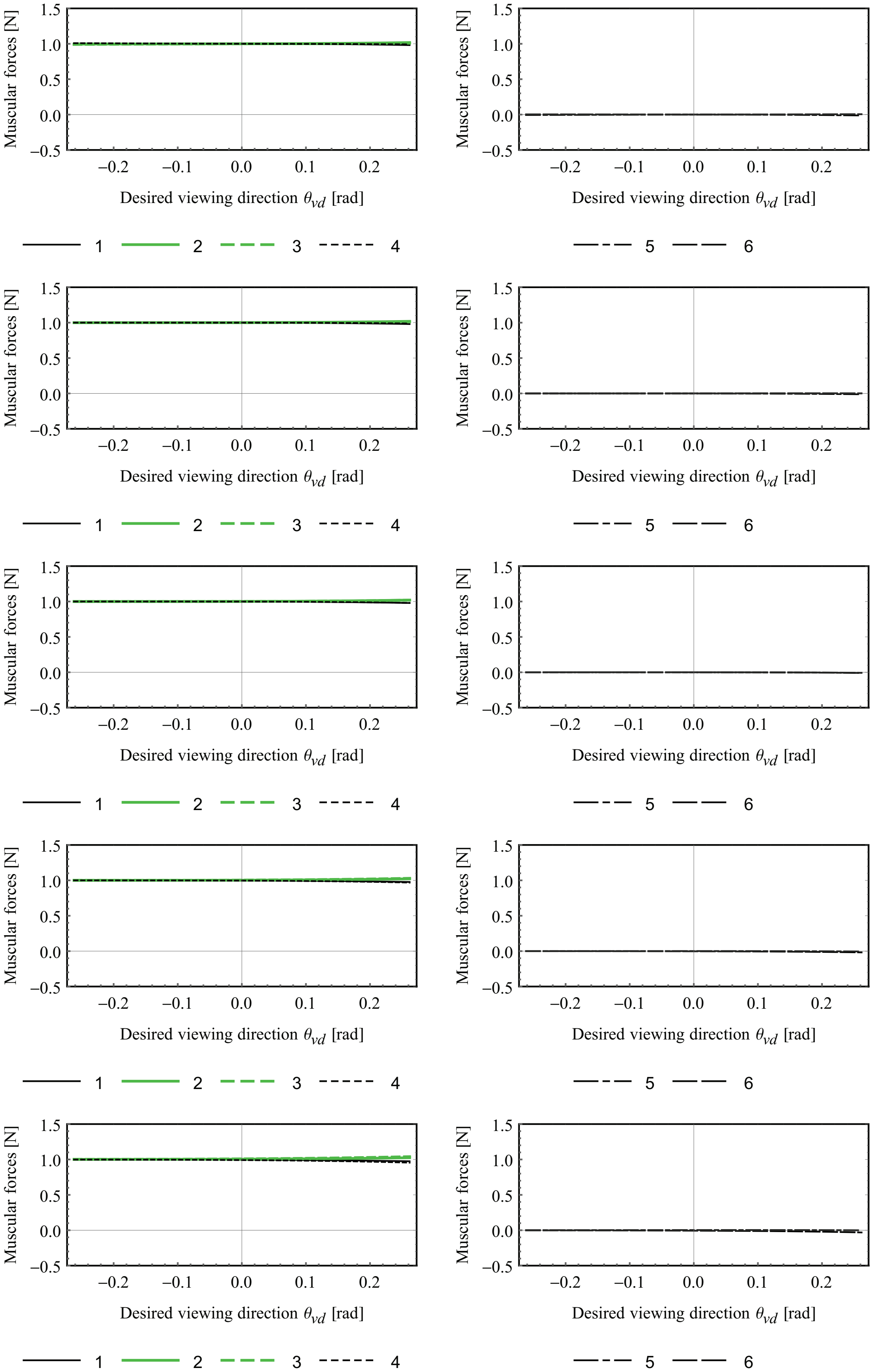

(a) Muscular forces of muscles 1 to 4

(b) Muscular forces of muscles 5 and 6

Fig. 6. Muscular forces according to $\boldsymbol{w}_{d14}$ (at $\gamma_d = 0.16$, 0.18, 0.20, 0.22, and 0.24 from the top row of the graphs).

Table 1. Forces of muscles i ($i = 1, \ldots, 4$) in $\boldsymbol{w}_{d14}$ at $\theta_{vd} = +\pi/12$.

muscle i	γ_d 0.16	0.18	0.20	0.22	0.24
$i = 1$	0.981	0.980	0.979	0.977	0.975
$i = 2$	1.02	1.02	1.02	1.02	1.02
$i = 3$	1.01	1.01	1.02	1.03	1.04
$i = 4$	0.992	0.988	0.980	0.969	0.955

* unit of the forces: [N]

Table 2. Kinetic parameters of the robot arm in the simulation.

Link p	Mass M_p [kg]	Distance to center of mass L_{Cp} [m]	Inertia I_p [kgm^2]
1	1.62	0.166	0.0673
2	0.96	0.104	0.0502

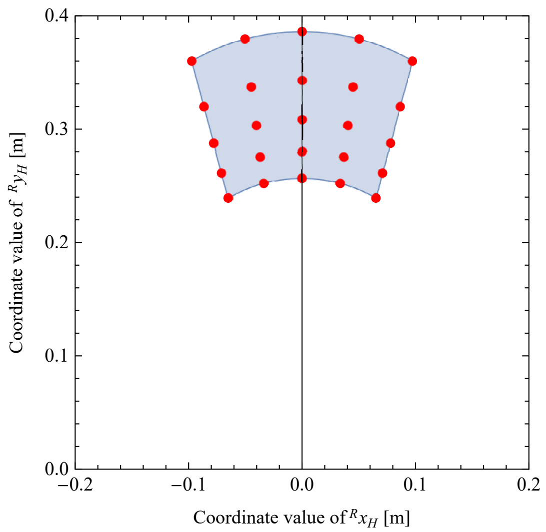

Fig. 7. Endtip points by the desired postures.

by dots, where the area framed by the lines indicates the calculation range.

However, the initial posture of the robot arm was fixed to $\boldsymbol{q}_I = [\ \pi/4 \quad \pi/4\ ]^T$ throughout the simulation.

7.2. Indices for Evaluating Control Performance

The settling time means the time necessary for the completion of the motion control and is usually used as a typical index for evaluating the response speed of a control method. The time measurement is started when the robot arm begins a motion at the initial posture and completed when the robot arm again comes to a stop at (or near) the desired posture. In the simulation, the robot arm was assumed to come to a stop if the absolute values of angular velocity and angular acceleration became less than 1.0×10^{-4} rad/s and 1.0×10^{-4} rad^2/s in all the joints.

However, it is noted that the stoppage of the robot arm described above does not necessarily mean the motion

Table 3. An example of simulation results ($\boldsymbol{w}_{da}$, $D = 10$).

Desired posture θ_{vd} [rad]	γ_d [rad]	Settling time [s]	Square error $\times 10^{-3}$ [rad^2]
−0.26	0.16	22.4	0.000
−0.13	0.16	21.3	0.000
0.00	0.16	22.3	0.000
0.13	0.16	25.1	0.000
0.26	0.16	27.5	0.000
−0.26	0.18	22.9	0.000
−0.13	0.18	22.6	0.000
0.00	0.18	22.3	0.000
0.13	0.18	25.1	0.000
0.26	0.18	27.0	0.000
−0.26	0.20	23.5	0.000
−0.13	0.20	25.8	0.000
0.00	0.20	25.2	0.000
0.13	0.20	24.2	0.000
0.26	0.20	25.7	0.000
−0.26	0.22	26.0	0.000
−0.13	0.22	25.4	0.000
0.00	0.22	21.2	0.000
0.13	0.22	23.3	0.000
0.26	0.22	22.7	0.000
−0.26	0.24	25.4	0.000
−0.13	0.24	24.2	0.000
0.00	0.24	20.3	0.000
0.13	0.24	20.2	0.000
0.26	0.24	19.4	0.000

control is successfully completed at the desired posture. This is especially true when the damping term in Eq. (17) accompanies a large value of D, as the motion of the robot arm in this case is in general very slow and easily slows down before sufficiently approaching a desired posture; therefore, it is necessary to consider the error of the posture at the stoppage of the motion from the desired posture as additional index for the evaluation of the control performance. Although the error can be measured in the joint angular, Cartesian, and binocular visual spaces, in this study, we measured it in the joint angular space and considered the square error for measuring the amount of error. The square error is defined by

$$\begin{aligned} \theta_{se} &= (\boldsymbol{\theta}_d - \boldsymbol{\theta}_s)^T (\boldsymbol{\theta}_d - \boldsymbol{\theta}_s) \\ &= (\theta_{d1} - \theta_{s1})^2 + (\theta_{d2} - \theta_{s2})^2, \quad \ldots \ldots \quad (18) \end{aligned}$$

where $\boldsymbol{\theta}_s = [\ \theta_{s1} \quad \theta_{s2}\ ]^T$ is the joint angle vector at the stoppage of the robot arm.

7.3. Example of Simulation Results and its Representation

An example of the simulation results is shown in **Table 3**, where $\boldsymbol{w}_{da}$ was used for mapping from $\boldsymbol{b}_d$ to $\boldsymbol{v}(\boldsymbol{\theta}_d)$ and $D = 10$ for calculating $\boldsymbol{D}$. Each row of **Table 3** indicates the desired posture expressed in the binocular visual space, the settling time, and the angular square error de-

Table 4. Averages and standard deviations of settling times.

Mapping	$\boldsymbol{w}_{da}$		$\boldsymbol{w}_{d56}$		$\boldsymbol{w}_{d14}$	
D [N·s/m]	Avg.	SD	Avg.	SD	Avg.	SD
3	68.8	5.5	67.7	5.0	124.7	86.3
5	41.8	3.2	41.5	2.8	282.2	272.1
7	30.5	2.8	30.4	2.3	390.9	354.6
10	23.6	2.2	24.5	2.0	472.5	400.4
15	32.5	5.1	35.6	3.6	494.3	317.8
20	43.0	6.5	46.9	4.4	589.1	395.0
25	52.8	7.8	57.5	5.3	678.2	468.7
30	62.2	9.0	67.5	6.1	700.1	431.3
35	71.2	10.2	77.2	6.9	722.0	418.4
40	80.0	11.3	86.7	7.6	776.8	461.2
45	88.5	12.4	95.8	8.3	829.6	500.6

* unit of the time: [s]

Table 5. Minimums, averages and maximums of square errors.

* unit of the square error: $\times 10^{-3}$ [rad^2]

D	$\boldsymbol{w}_{da}$ Min.	$\boldsymbol{w}_{da}$ Avg.	$\boldsymbol{w}_{da}$ Max.	$\boldsymbol{w}_{d56}$ Min.	$\boldsymbol{w}_{d56}$ Avg.	$\boldsymbol{w}_{d56}$ Max.
3	0.000	0.000	0.000	0.000	0.000	0.000
5	0.000	0.000	0.000	0.000	0.000	0.000
7	0.000	0.000	0.000	0.000	0.000	0.000
10	0.000	0.000	0.000	0.000	0.000	0.000
15	0.000	0.000	0.001	0.000	0.000	0.001
20	0.000	0.001	0.001	0.000	0.001	0.001
25	0.000	0.001	0.002	0.000	0.001	0.002
30	0.000	0.001	0.003	0.001	0.002	0.003
35	0.000	0.002	0.004	0.001	0.002	0.004
40	0.001	0.003	0.005	0.001	0.003	0.005
45	0.001	0.003	0.006	0.001	0.004	0.006

D	$\boldsymbol{w}_{d14}$ Min.	$\boldsymbol{w}_{d14}$ Avg.	$\boldsymbol{w}_{d14}$ Max.
3	0.000	0.766	6.970
5	0.000	0.999	7.131
7	0.000	1.265	8.451
10	0.001	2.110	10.948
15	0.001	5.260	27.369
20	0.003	6.571	37.673
25	0.004	7.671	44.650
30	0.006	10.299	50.443
35	0.008	12.553	55.553
40	0.011	13.861	60.200
45	0.014	15.060	64.502

fined by Eq. (18).

The conditions given for the motion control were the combinations of the mapping (using $\boldsymbol{w}_{da}$, $\boldsymbol{w}_{d56}$, and $\boldsymbol{w}_{d14}$) and the value of D (3, 5, 7, 10, 15, 20, 25, 30, 35, 40, 45 N·s/m); therefore, the number of the results for these conditions was 33, including the result shown in **Table 3**. However, the direct observations or comparisons of the 33 results based on the table form as shown in **Table 3** are probably meaningless or provide few suggestions; therefore, we consider the representation of the result for each condition by statistical values.

For the settling time, the average and standard deviation throughout all the desired postures are used. In the case of the results shown in **Table 3**, they are 23.6 ± 2.2 s. However, the average, maximum, and minimum are chosen for the square error, and all these are 0.000×10^{-3} rad^2 in the case of the results in **Table 3**. Here, it is noted that using the standard deviation instead of the maximum and minimum is considered inappropriate, because a normal (or Gaussian) distribution cannot be assumed for the square error because of its absoluteness given by Eq. (18).

7.4. Observation of the Settling Time

Table 4 shows the comparison of the settling times among the mappings. The left-most column of the table shows the values of D for the calculation of the matrix $\boldsymbol{D}$. The remaining columns show the average and standard deviation for each of the mappings by $\boldsymbol{w}_{da}$, $\boldsymbol{w}_{d56}$, and $\boldsymbol{w}_{d14}$.

A major observation from **Table 4** is that the smallest averages and standard deviations are obtained at $D = 10$ in the mappings of $\boldsymbol{w}_{da}$ and $\boldsymbol{w}_{d56}$. A second observation found from this comparison is that the average of the mapping $\boldsymbol{w}_{da}$ becomes smaller than that of $\boldsymbol{w}_{d56}$ when D increases, whereas the standard deviation of $\boldsymbol{w}_{da}$ becomes larger than that of $\boldsymbol{w}_{d56}$. This observation suggests that the performances of motion control by the mappings of $\boldsymbol{w}_{da}$ and $\boldsymbol{w}_{d56}$ are similar but different. A statistical test (t-test) showed that the difference in the averages of the two mappings is significant with a significance level of 1% at all D larger than 15 N·s/m.

It is also necessary to pay particular attention to the observation that the average and standard deviation of the mapping $\boldsymbol{w}_{d14}$ is much larger than those of the other two mappings. The t-test shows that the differences in the averages between the mapping of $\boldsymbol{w}_{d14}$ and each of the other two mappings are very significant, with a significance level of 0.1%.

The assumption previously described in Section 6.1 is that the feature of the analogous dependence of $\boldsymbol{v}(\boldsymbol{\theta}_d)$ on $\boldsymbol{b}_d$ in the mappings of $\boldsymbol{w}_{da}$ and $\boldsymbol{w}_{d56}$ provides a similar control performance to those mappings, and the weak dependence of $\boldsymbol{v}(\boldsymbol{\theta}_d)$ on $\boldsymbol{b}_d$ in the mapping of $\boldsymbol{w}_{d14}$ negatively contributes to the control performance obtained by the mapping. According to the observations in this subsection, this assumption is considered reasonable.

7.5. Observation of the Square Error

The upper table in **Table 5** shows the minimums, averages, and maximums of the square errors obtained using the mappings of $\boldsymbol{w}_{da}$ and $\boldsymbol{w}_{d56}$, and the lower table shows those obtained from the mapping of $\boldsymbol{w}_{d14}$. The observation common to the three mappings is that all the minimums, averages, and maximums increase as the value of D increases; however, this is naturally understood, because the robot arm slowed and satisfied the stoppage condition described in Section 7.2 before sufficiently approaching a desired posture when muscular damping was provided by a large value of D.

However, observation of the minimums, averages, and maximums for the same value of D reveals that these values, especially the average and maximum, for the mapping using $\boldsymbol{w}_{d14}$ are considerably larger than those for the mappings using $\boldsymbol{w}_{da}$ and $\boldsymbol{w}_{d56}$. For each value of D, a statistical test (Mann-Whitney U-test or Wilcoxon rank-sum test) showed that there is no significant difference between the averages of the mappings $\boldsymbol{w}_{da}$ and $\boldsymbol{w}_{d56}$, whereas the average of the mapping $\boldsymbol{w}_{d14}$ is significantly different from those of $\boldsymbol{w}_{da}$ and $\boldsymbol{w}_{d56}$ with a significance level of 1%. The differences described above are also considered reasonably acceptable for the same reason as that described in the final paragraph of the previous subsection (Section 7.4).

8. Conclusion

This paper addressed a two DOF planar robot arm antagonistically actuated by six muscles (four monoarticular muscles and two biarticular muscles). The robot arm considered has no pulleys on its joints, and the muscles are directly connected to anchoring points on the links. This muscular structure enables PTP motion control of the robot arm in a feedforward manner, without using any sensors for measuring the motion of the joints or muscles. This is an advantageous feature of the robot arm discussed.

A desired posture of the robot arm can be described by two variables, whereas the number of the muscles is six. Therefore, the robot arm considered in this paper is redundant, and there exist many combinations of muscular forces that allow it to arrive at the desired posture. This paper addressed the issue of redundancy by considering the following two viewpoints: the expression of a desired posture in the binocular visual space and the consideration of three characteristic mappings from the desired posture to the muscular forces.

An analysis by means of numerical calculations revealed that two of the three mappings ($\boldsymbol{w}_{da}$ and $\boldsymbol{w}_{d56}$) implemented provided almost the same dependence property of muscular forces on the desired postures; however, the dependence property of the third mapping ($\boldsymbol{w}_{d14}$) was very weak. Based on these analysis results, it was assumed in this study that the strengths of the dependencies affected the performances of the PTP motion control to the desired postures. An investigation by means of simulating the motion control of the robot arm showed that the above assumption is reasonably acceptable; that is, the mappings with the dependencies on the desired posture ($\boldsymbol{w}_{da}$ and $\boldsymbol{w}_{d56}$) exhibited similar control performances (although they were statistically different), and these performances were much better than that obtained by the mapping with less dependency on the desired posture ($\boldsymbol{w}_{d14}$).

In the authors' opinion, the results described in the previous paragraph suggest means for developing motion control of a robot arm antagonistically actuated by monoarticular and biarticular muscles. However, an approach or a method that can be proposed for this development from an engineering point of view has not currently been found, and this is an important future issue regarding the study in this paper. It is thought that the key for such an approach or method is the mapping of $\boldsymbol{w}_{d14}$, which is less dependent on (or almost independent of) the desired postures of the robot arm. It is reasonably understood from the observations described in this paper that the mapping alone is incapable of improving the motion control performance; however, the lower dependency of the mapping on the desired postures is also considered to be useful for arbitrary adjustment of the muscular forces for motion control to a desired posture, provided that the mapping is combined with an additional mapping that has dependency on the desired postures ($\boldsymbol{w}_{d56}$, for example). If we can devise an idea for using the scheme mentioned above from an engineering viewpoint, in the context of the method proposed in [12], for example, the calculation of the feedforward control input for a desired posture $\boldsymbol{b}_d$ by $\beta_{14}\boldsymbol{w}_{d14} + \beta_{56}\boldsymbol{w}_{d56}$ can be considered, under adjusting the coefficients β_{14} and β_{56} in accordance with the criterion of avoiding actuator saturation.

An additional future issue is the investigation of the dependence properties of the mappings for a wider calculation range of desired postures in the binocular visual space. The investigation of the kinematic arrangements of the robot arm and the "eyes" for constituting a binocular visual space, which do not resemble the arrangement of humans, is also an interesting future topic. Toward engineering applications of the method suggested in this paper, the visual binocular space should be extended from two to three dimensions, using a robot arm capable of three-dimensional motion.

References:

[1] G. J. V. I. Schenau, "From rotation to translation: Constraints on multi-joint movements and the unique action of bi-articular muscles," Human Movement Science, Vol.8, No.4, pp. 301-337, 1989.

[2] T. Oshima, N. Momose, K. Koyanagi, T. Matsuno, and T. Fujikawa, "Jumping mechanism imitating vertebrate by the mechanical function of bi-articular muscle," 2007 Int. Conf. on Mechatronics and Automation, pp. 1920-1925, August 2007.

[3] T. Kaneko, K. Ogata, S. Sakaino, and T. Tsuji, "Impact force control based on stiffness ellipse method using biped robot equipped with biarticular muscles," 2015 IEEE/RSJ Int. Conf. on Intelligent Robots and Systems (IROS), pp. 2246-2251, September 2015.

[4] Y. Nakata, A. Ide, Y. Nakamura, K. Hirata, and H. Ishiguro, "Hopping by a monopedal robot with a biarticular muscle by compliance control – an application of an electromagnetic linear actuator –," J. Robot. Mechatron., Vol.25, No.1, pp. 106-114, 2013.

[5] M. Kumamoto, T. Oshima, and T. Yamamoto, "Control properties induced by the existence of antagonistic pairs of bi-articular muscles – mechanical engineering model analyses," Human Movement Science, Vol.13, No.5, pp. 611-634, 1994.

[6] V. Salvucci, Y. Kimura, S. Oh, and Y. Hori, "Force maximization of biarticularly actuated manipulators using infinity norm," IEEE/ASME Trans. on Mechatronics, Vol.18, No.3, pp. 1080-1089, June 2013.

[7] T. Baratcart, V. Salvucci, and T. Koseki, "Experimental verification of two-norm, infinity-norm continuous switching implemented in resolution of biarticular actuation redundancy," Advanced Robotics, Vol.29, No.19, pp. 1243-1252, 2015.

[8] K. Tahara, Y. Matsutani, D. Nakagawa, M. Sato, and H. Kino, "Variable combination of feed-forward and feedback manners for set-point control of a musculoskeletal arm considering the maximum exertable muscular force," IECON 2016 – 42nd Annual Conf. of the IEEE Industrial Electronics Society, pp. 815-820, Octber 2016.

[9] V. Salvucci, Y. Kimura, S. Oh, and Y. Hori, "Biwi: Bi-articularly actuated and wire driven robot arm," 2011 IEEE Int. Conf. on Mechatronics, pp. 827-832, April 2011.

[10] T. Oshima, T. Fujikawa, and M. Kumamoto, "Control of elasticity and trajectory of robot arm with redundant actuators," J. Robot. Mechatron., Vol.14, No.3, pp. 253-261, 2002.

[11] H. Kino, S. Kikuchi, Y. Matsutani, K. Tahara, and T. Nishiyama, "Numerical analysis of feedforward position control for non-pulley musculoskeletal system: a case study of muscular arrangements of a two-link planar system with six muscles," Advanced Robotics, Vol.27, No.16, pp. 1235-1248, 2013.

[12] Y. Matsutani, K. Tahara, H. Kino, and H. Ochi, "Complementary compound set-point control by combining muscular internal force feedforward control and sensory feedback control including a time delay," Advanced Robotics, Vol.32, No.8, pp. 411-425, 2018.

[13] T. Oshima, T. Fujikawa, and M. Kumamoto, "Coordination control of arm using antagonistic actuators," J. Robot. Mechatron., Vol.14, No.3, pp. 270-277, 2002.

[14] T. Morizono, K. Tahara, and H. Kino, "Experimental investigation of contribution of biarticular actuation to mappings between sensory and motor spaces," IECON 2015 – 41st Annual Conf. of the IEEE Industrial Electronics Society, pp. 3573-3578, November 2015.

[15] T. Morizono, K. Tahara, and H. Kino, "A study on effect of biarticular muscles in an antagonistically actuated robot arm through numerical simulations," Artificial Life and Robotics, Vol.22, No.1, pp. 74-82, 2017.

[16] H. Okada, M. Ae, N. Fujii, and Y. Morioka, "Body segment inertia properties of Japanese elderly," Biomechanisms, Vol.13, pp. 125-139, 1996 (in Japanese).

Supporting Online Materials:

[a] Japanese Body Dimension Data 1991-92 (Japanese pages only). https://www.dh.aist.go.jp/database/91-92/index.html [Accessed April 11, 2017]

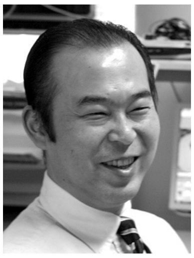

Name:
Tetsuya Morizono

Affiliation:
Professor, Department of Information and Systems Engineering, Faculty of Information Engineering, Fukuoka Institute of Technology

Address:
3-30-1 Wajiro-Higashi, Higashi-ku, Fukuoka City, Fukuoka 811-0295, Japan

Brief Biographical History:
1998- Research Associate, Toyota Technological Institute
2007- Associate Professor, Fukuoka Institute of Technology
2017- Professor, Fukuoka Institute of Technology

Main Works:
- "A study on effect of biarticular muscles in an antagonistically actuated robot arm through numerical simulations," Artificial Life and Robotics, Vol.22, No.1, pp. 74-82, 2017.
- "Evaluating Wearing Mobility of Wearable Robot Mechanisms Based on Measurement," Int. J. of Space-Based and Situated Computing, Vol.6, No.4, pp. 209-220, 2016.
- "Operational "Feel" Adjustment by Reinforcement Learning for a Power-Assisted Positioning Task," Int. J. Automation Technol., Vol.3, No.6, pp. 671-680, 2009

Membership in Academic Societies:
- The Japan Society of Mechanical Engineers (JSME)
- The Robotics Society of Japan (RSJ)
- The Virtual Reality Society of Japan (VRSJ)

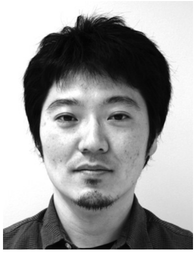

Name:
Kenji Tahara

Affiliation:
Associate Professor, Department of Mechanical Engineering, Faculty of Engineering, Kyushu University

Address:
744 Moto'oka, Nishi-ku, Fukuoka City, Fukuoka 819-0395, Japan

Brief Biographical History:
2003- Research Scientist, Institute of Physical and Chemical Research (RIKEN)
2007- Research Associate Professor, Faculty of Information Science and Electrical Engineering, Kyushu University
2011- Associate Professor, Faculty of Engineering, Department of Mechanical Engineering, Kyushu University

Main Works:
- "Feedforward control of twisted and coiled polymer actuator based on a macroscopic nonlinear model focusing on energy," IEEE Robotics and Automation Letters, Vol.3, Issue 3, pp. 1824-1831, 2018.
- "Modeling framework for macroscopic dynamics of twisted and coiled polymer actuator driven by Joule heating focusing on energy and convective heat transfer," Sensors and Actuators, A: Physical, Vol.267, pp. 443-454, 2017.
- "Grasp and dexterous manipulation of multi-fingered robotic hands: a review from a control view point," Advanced Robotics, pp. 1-21, 2017.

Membership in Academic Societies:
- The Institute of Electrical and Electronics Engineers (IEEE)
- The Robotics Society of Japan (RSJ)
- The Japan Society of Mechanical Engineers (JSME)

Name:
Hitoshi Kino

Affiliation:
Professor, Department of Intelligent Mechanical Engineering, Faculty of Engineering, Fukuoka Institute of Technology

Address:
3-30-1 Wajiro-Higashi, Higashi-ku, Fukuoka City, Fukuoka 811-0295, Japan

Brief Biographical History:
1994 Received B.S. in Engineering from Ritsumeikan University
1996 Received M.S. in Engineering from Ritsumeikan University
2000 Received Ph.D. in Engineering from Ritsumeikan University
2011- Professor, Fukuoka Institute of Technology

Main Works:
- "Sensorless Point-to-point Control for a Musculoskeletal Tendon-driven Manipulator – Analysis of a Two-DOF Planar System with Six Tendons –", Advanced Robotics, Vol.31, No.16, pp. 851-864, 2017.
- "Inverse Dynamics of Human Passive Motion Based on Iterative Learning Control," IEEE Trans. on Systems, Man, and Cybernetics, part A, Vol.42, No.2, pp. 307-315, 2012.
- "Sensorless Position Control Using Feedforward Internal Force for Completely Restrained Parallel-wire Driven Systems," IEEE Trans. on Robotics, Vol.25, No.2, pp. 467-474, 2009.

Membership in Academic Societies:
- The Robotics Society of Japan (RSJ)
- The Japan Society of Mechanical Engineers (JSME)
- The Institute of Electrical and Electronics Engineers (IEEE)